Supplementary information

Preclinical safety assessment of red emissive gold nanocluster conjugated crumpled MXene nanosheets: A dynamic duo for image-guided photothermal therapy

Barkha Singh[a.b.], Rohan Bahadur[a], Priyanka Maske[a], Mayuri Gandhi[b], Dipty Singh[c]*, Rohit Srivastava[a*]

a- Department of Biosciences and Bioengineering, Indian Institute of Technology (IIT) Bombay, Powai, Mumbai, 400076, India

b- Centre for Research in Nano Technology & Science (CRNTS), Indian Institute of Technology (IIT) Bombay, Powai, Mumbai, 400076, India

c- National Institute for Research in Reproductive and Child Health (NIRRCH), Parel, Mumbai, 400012,India

Characterization/ Spectroscopic investigations

Morphological characterization and elemental mapping were done using transmission electron microscopy (TEM 200 kV- JEOL JEM 2100F) imaging and scanning electron microscopy (SEM- JEOL, JSM 7600F) imaging. Size distribution was measured using Image-J software. Atomic force microscopy (AFM) (Bruker, Multimode Nanoscope-IV) was used to measure the lateral thickness of the nanomaterial. Crystallinity of the nanosheets was studied using High resolution X-ray diffraction (Smartlab, Rigaku diffractometer). XRD was recorded in the range of 5-80^{o}. Fourier-Transform Infrared Spectroscopy (3000 Hyperion Microscope with Vertex 80 FTIR System) was done of powdered sample to study the chemical properties of the material by mixing it with KBr in the ratio of ~1:200. X-ray photoelectron spectroscopy (XPS) of the nanomaterial was done using (Kratos Analytical, AXIS Supra). A drop of material was dried on the aluminium foil for the analysis.

Absorbance was recorded using UV-vis spectroscopy (PerkinElmer Lamda-25) while photoluminescence was checked using photoluminescence spectroscopy (Hitachi F-2500). The photoluminescence was checked visually by irradiating the sample under UV light in a Perkin-Elmer Geliance 1000 gel-Doc system and pictures taken using a cell phone camera. Contact angle of FA_Au@c-Ti_3C_2 (500 µg mL^{-1}) was recorded using contact angle meters (Apex Instruments). The sample dispersion was checked in various solvents. The FA_Au@c-Ti_3C_2 was dispersed in Milli-Q, PBS, Complete DMEM, methanol, ethanol, isopropyl alcohol, acetic acid, ethyl acetate, dimethylformamide, dimethyl sulfoxide, acetone, acetonitrile, dichloromethane to make the final concentration of 1mg mL^{-1}.

For stability study the FA_Au@c-Ti_3C_2 was dispersed in Milli-Q, PBS, Complete DMEM and kept in a shaker at 37^{O}C. The digital images were captured at different time points up to 5 days.

***In vitro* cytotoxicity assays:**

Fibroblast cell line (L929) and cancer cell line (MDAMB-231) were cultured in Dulbecco's Modified Eagle Medium (DMEM) supplemented with 1% v/v antibiotic and 10% Fetal bovine serum incubated at 5% CO_2 and 37 °C in a humidified condition.

Alamar blue assay was used to monitor cell viability. Cells were seeded in 96 well plate and allowed to adhere. The nanomaterial at various concentrations was added and incubated for 24 hours. The cells were washed with PBS and resazurin dye was added and incubated for 4 hours. Untreated cells were taken as negative control (NC), Triton-X 100 treated cells as positive control while resazurin dye dispersed in DMEM was considered as the media blank. The

intensity of absorbance and fluorescence was measured using a plate reader (TECAN Infinite 200 PRO series). Cell viability was calculated using the following equation.

$$Cell\ viability\ (\%) = \left[\frac{Intensity\ of\ sample - Intensity\ of\ media\ blank}{Intensity\ of\ NC - Intensity\ of\ media\ blank}\right] X\ 100$$

The effect of FA_Au@c-Ti_3C_2 on L929 cellular proliferation was studied using Cell Cycle Flow Cytometry Assay. The cells were attached on 6 well plates and FA_Au@c-Ti_3C_2 (100 and 250 µg mL^{-1}) was incubated for 24 hr. Cells were washed with PBS, harvested using trypsin and centrifuged. The pellet was fixed with chilled 70% ethanol dropwise and incubated for 30 minutes at 4°C. The cells were again centrifuged, resuspended and then incubated with RNAse (50 µL of 100µg mL^{-1}) and propidium iodide (200µl from 50µg mL^{-1}) and analyzed using Flow cytometry. G1, S, and G2 populations were resolved using FlowJo software.

THP-1 cells differentiated macrophage-like cells: THP-1 cells were cultured in RPMI-1640 media and were sub cultured at $8x10^5$ cells mL^{-1}. THP-1 cells were seeded in a 96 well plate. THP-1 differentiation was done using 25 ng mL^{-1} phorbol 12-myristate-13-acetate (PMA) and incubated for 24 hours. The differentiated macrophages were washed with PBS and fresh media was added. Cells were kept in incubator for the next 24 hours. Different concentrations of nanomaterials were added to macrophages and incubated for another 24 hours. The cells were washed with PBS and resazurin dye was added. The intensity of absorbance and fluorescence was measured using a plate reader after 4 hours of incubation.

Microscopic image of FA_Au@c-Ti_3C_2 treated L929 cells: The effect of FA_Au@c-Ti_3C_2 on the morphology of L929 cells were observed using Environmental Scanning Electron Microscope (ESEM). L929 cells were cultured and allowed to adhere on glass coverslips. The cells were treated with nanosheets (25, 150, 250 µg mL^{-1}) for 24 hr and then washed with 1XPBS. Cells were fixed using 4% paraformaldehyde. The cells were dehydrated using ethanol gradient (50%-100%) for 10 min each at room temperature and then allowed to air dry. The coverslips were then observed under ESEM.

Hemolysis assay: Hemocompatibility of FA_Au@c-Ti_3C_2 was tested using blood obtained from healthy participants with their agreement and clearance from the Institutional Ethics Committee (IEC), IIT Bombay (No.IITB-IEC/2019/031). The collected whole blood was

diluted with PBS and centrifuged for 5 minutes at 1000 rpm, with the pellet resuspended in PBS. Multiple centrifugations and redispersion cycles were performed until the supernatant was clear and free of all other components except RBCs. FA_Au@c-Ti_3C_2 in various concentrations (50-1000 µg mL^{-1}) were added to 200 µL equal volume of isolated RBCs. Triton X-100 treated RBCs was taken as positive control (PC) while PBS treated RBCs were considered as negative control (NC). All the samples were centrifuged for 5 minutes at 4000 rpm after 2 hours of incubation at 37 °C. Digital images of pellet were taken. Supernatant was carefully withdrawn into a 96-well plate and its absorbance was measured at 540 nm with a plate reader. PBS was taken as media blank. The hemolysis % was calculated using the following equation:

$$Hemolysis\ (\%) = \left[\frac{Intensity\ of\ sample - Intensity\ of\ media\ blank}{Intensity\ of\ PC - Intensity\ of\ media\ blank}\right] X\ 100$$

The morphology of RBCs was observed under ESEM. The RBCs were fixed using 2% glutaraldehyde overnight at 4 ℃. The cells were washed with PBS and drop casted on aluminium foil. The sample was observed under ESEM.

***In vivo* toxicity:**

The animal experimentation was performed at ICMR- National Institute for Research in Reproductive and Child Health (ICMR-NIRRCH). The ethical permission for the same was obtained prior to conducting the experiment (IAEC no: 12/21). The animal experimentation was performed in accordance with the guidelines of Committee for the Purpose of Control and Supervision of Experimental Animals (CPCSEA), India.

Adult 6–8-week-old male and female Wistar rats with 250 ± 50 g body weight were used to study the acute toxicity as per OECD guideline 425. These animals were maintained in controlled environment at a temperature of 23 ± 1°C, humidity of 55 ± 5 %, and 14 hr light/10 hr dark cycle. Soy-free in-house prepared pellets and sterilized water was provided to these animals' ad-libitum.

The male and female Wistar rats were divided in two groups (n=16/group) consisting of vehicle control (0.01M PBS) and treatment (FA_Au@c-Ti_3C_2). A single dose of the treatment (20mg kg^{-1}) was administered to the animals by oral gavage/I.V. injection according to the body weight of the animals. [The dose was decided based on the previous reported literature on MXene based biomaterial].These rats were monitored for clinical signs of mortality or toxicity for 24 hours and further weekly body weights were monitored till 14 days.

Blood bio-chemistry and hematology: On 14th day, the terminal blood was collected from retro-orbital route in heparinized tubes for hematology analysis and in non-heparinized tubes for serum separation (blood centrifuged at 6000 rpm for 15 min); the serum after separation were stored at -20°C till analysis. The hematology checked Hemoglobin, Red blood cells, White blood cells, Platelets, Neutrophils, Eosinophils, Lymphocytes, Monocytes, Packed cell volume, mean corpuscular volume, mean corpuscular hemoglobin, Mean Corpuscular Hemoglobin Concentration values. The serum biochemistry analysis was done by comparing parameters like Serum Glutamic Pyruvic Transaminase (SGPT), Serum Glutamic Oxaloacetic Transaminase (SGOT), Phosphate, Direct Bilirubin, Total Bilirubin, Creatinine, Glucose, Triglycerides, Cholesterol, High Density Lipoprotein Concentration, Uric Acid, Calcium, Albumin, and Total Protein.

Coefficient of organ to body weight: Individual weights of animals were determined shortly before the FA_Au@Ti_3C_2 is administered and at 7th and 14th day post treatment. At the end of the study animals were weighed and euthanized.

Organs such the Brain, Heart, Liver, Lungs, Kidney, Adrenal gland, Hypothalamus, Pituitary, Spleen, Testis, Seminal Vesicles, Prostate, Epididymis of the male rats were promptly removed and weighed. For female rats organs like Brain, Heart, Liver, Lungs, Kidney, Adrenal gland, Hypothalamus, Pituitary, Spleen, Uterus and Ovaries were removed and weighed.

The coefficients of organs weight to body weight were computed as the ratio of tissue wet weight (g) to body weight (g).

Histopathology: Tissues were processed for histopathology as per the standard protocol[1]. Briefly, tissues were fixed in 4 % formalin, embedded in paraffin, and sectioned manually with a microtome to produce 4–5 μm-thick paraffin slices. Hematoxylin and eosin(H&E) were used to stain dewaxed sections and then observed under light microscope. The images were captured using Microscope (DM2000 LED, Leica, USA)

Cellular Imaging and cell uptake of FA_Au@c-Ti_3C_2:

The qualitative uptake was studied using confocal microscopy. MDAMB-231 cells were seeded in a 24 well plate on a coverslip and allowed to attach. FA_Au@c-Ti_3C_2 was added to the cells and incubated for 24 hours. Cells were washed with PBS and fixed using 4 % paraformaldehyde. Cell nucleus was labelled with DAPI dye (4′,6-diamidino-2-phenylindole). The coverslip was mounted on a slide and observed under confocal microscope.

The quantitative uptake was studied using Inductively Coupled Plasma Atomic Emission Spectroscopy (ICP-AES). The cells were seeded on 6 well plate and allowed to adhere. MDAMB-231 cells were treated with FA_Au@c-Ti_3C_2 at various time points of 1, 2, 4, 6, 8, 12 hours. The cells were then trypsinized, centrifuged and the pellet was digested using aqua regia overnight. The dispersion was then diluted and ICP-AES was carried out for the quantification of Titanium.

Uptake study using AFM: The interaction of nanomaterial and MDAMB-231 cells were observed using Bio- atomic force microscope facility (Model: Asylum Research, USA. MFP-3D BIO). Cells were seeded on coverslip and allowed to adhere. The cells were then treated with Au@c-Ti_3C_2 and FA_Au@c-Ti_3C_2 for 24 hours. Cells were then washed with PBS and fixed using 4% paraformaldehyde. The fixed cells were dehydrated using ethanol gradient and then observed under AFM. The height was calculated by drawing a straight line on the cytoplasm and nuclear region respectively (WSxM software). The roughness of the cells was evaluated using Asylum research AFM software. A box size of 20µm was drawn over cytoplasm and nucleus region respectively and then roughness was calculated using 'Calculate roughness' pre-installed function. Roughness was plotted using RMS/surface area.

Photothermal Transduction and *in-vitro* photothermal cytotoxicity:

100 µL aliquots of FA_Au@c-Ti_3C_2 nanoparticles (100, 200 µg mL^{-1}) was taken in 96-well plates maintained at 37 °C in a water bath. Each sample was exposed to an 808 nm NIR laser for up to 10 minutes. A digital thermometer was used to track the temperature at various intervals. The photothermal stability of FA_Au@c-Ti_3C_2 nanoparticles was evaluated by heating the sample for 5 cycles and recording the rise in temperature.

MDAMB-231 cells were used to evaluate the *in-vitro* photothermal cytotoxicity of FA_Au@c-Ti_3C_2 nanoparticles. Cells were seeded on a 96 well plates and allowed to attach. The cells were washed and nanomaterials containing 20, 30, and 40 ppm of Ti were added. After 24 hr incubation, the laser irradiation for 10 minutes was done using 808 nm laser system. The cells were kept in incubator overnight following which alamar assay was performed. For laser irradiation time-dependent cytotoxicity same protocol was followed except laser was irradiated for 3,5,7,10 minutes with cells incubated with 40 ppm of titanium.

Cell Apoptosis Using Annexin V-FITC and PI Staining:

MDAMB cells were seeded in 96-well plate and incubated overnight. Fresh media containing 40 ppm of FA_Au@c-Ti_3C_2 nanoparticles were added to the cultured medium. After 24-hour incubation period, the cells were washed three times with PBS, after which fresh media was added, and irradiated for 10 minutes with an 808 nm NIR laser for 10 minutes. Cells were stained with annexin V-FITC and PI after a 12-hour incubation period (Following the manufacturer's procedure, BD Biosciences). Microscope was used to visualize the cells under FITC and PI filter in Zeiss spinning disc microscopy in the live cell imaging chamber. The same procedure was followed with cells (NC), cells + laser only, cells+nanoparticles, cells +triton-X100 (PC) for the comparison.

Effect of PTT on cancer cells proliferation and ROS generation:

MDAMB cells were seeded in 6-well plate and incubated overnight. Fresh media containing FA_Au@c-Ti_3C_2 nanoparticles were added to the cultured medium. After 24-hour incubation period, the cells were washed three times with PBS, trypsinized and irradiated with an 808 nm NIR laser for 10 minutes. The cells were then again added to in 6 well plate and allowed to attach overnight. Cells were washed with PBS, harvested using trypsin and centrifuged. The obtained pellet was then fixed using chilled 70 % ethanol dropwise. The cells were then fixed for 30 min at 4^{o}C. The cells were again centrifuged, resuspended and then incubated with RNAse (50 µL of 100µg mL-1) and propidium iodide (200µl from 50µg mL-1) and analyzed using Flow cytometry. G1, S, and G2 populations were resolved using FlowJo software.

For ROS study, MDAMB cells were seeded in 6-well plate and incubated overnight. Fresh media containing FA_Au@c-Ti_3C_2 nanoparticles were added to the cultured medium. After 24-hour incubation period, the cells were washed three times with PBS, trypsinized and irradiated for 1,3, and 10 minutes respectively with an 808 nm NIR laser. The cells were then incubated with 5 µM dichlorodihydrofluorescein diacetate (DCFDA) dye for 30 minutes in dark. The cells were washed again and analyzed using Flow cytometry in FITC filter. In a control experiment the same procedure was followed on untreated MDAMB cells, cells treated with laser only and cells treated with nanoparticles only. H_2O_2 was used as the positive control.The data was analysed using FlowJo software.

Table S1 Recent reported literature on MXene Gold composite

S.No	MXene-composite	MXene size and property	Size and property	Salient feature	Application	Reference
1	Gold nanoparticle/MXene	Accordion-like architecture of MXene	5 nm gold nanoparticles	Synergetic boost the electrochemical signals by ~ 4 times	Sensitive and rapid detection of multiple miRNAs in total plasma	[2]
2	Core–shell nanocomposites (Ti_3C_2@Au)	Ti_3C_2 nanosheets with a size of ~200 nm	Au nanoparticles shell with the thickness of ~30 nm	Excellent synergistic effect, absorbance NIR-I and NIR-II biological windows. Improved stability and the biocompatibility of the Ti_2C_3@Au nanocomposites by the thiol group	Enhanced photo–radio combined therapy	[3]
3	Gold nanoclusters (AuNCs) on MXene nanosheets.	Nanosheets size ≈0.9 μm	< 2 nm	Synergistic antimicrobial with low ic_{50} values of 11.7 μg ml^{-1} of MXene and 0.04 μm of AuNCs.	Bacterial death of both gram-positive and gram-negative bacteria	[4]
4	MXene ($Ti_3C_2T_x$) nanosheets and gold nanorods (AuNRs)	-	Average length - 49.3 nm, average transverse diameter- 9.7 nm	SERS substrate, excellent SERS sensitivity	Organic pollutants sensing	[5]
5	MXene nanosheets and gold nanoparticles	Lateral size is 2–3 μm	50 nm	Enhanced printability and conductivity of 2% GelMa , improved the rheological properties of the hydrogel	Biocomposite inks	[6]
6	Titanium carbide Ti_3C_2Tx (MXene) and gold	Few layered $Ti_3C_2T_x$	35–40 nm	Template for the high electrocatalyti	Uric acid, and Folic Acid at physiologicalp	[7]

	nanoparticles	flakes		c activity of the analytes, excellent electro-catalytic performance	H sensing	
7	Au@MXene	Around 2–3 µm	40–50 nm	Surface-Enhanced Raman spectroscopy (SERS)	Highly sensitive SERS detection of methylene blue (mb) ,	[8]
8	Au/MXene and Au/Fe_3O_4/MXene		5-10 nm	Lower acute toxicity	Photothermal therapeutic effects	[9]
9	**Gold nanoclusters on Crumpled MXene sheets**	**under 400 nm**	**<5 nm**	**Red emissive and PTT**	**Image guided PTT**	**This work**

Results and Discussions:

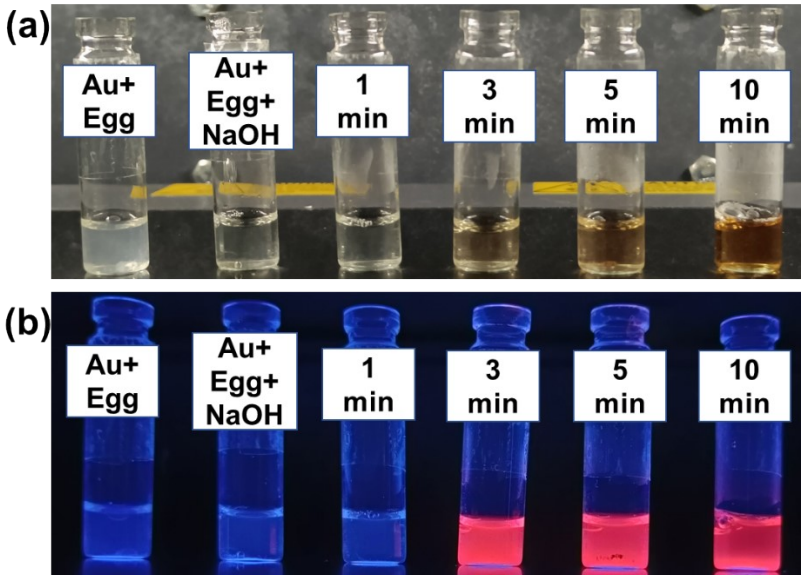

Figure S1: Digital image of au salt+egg white, Au salt+eggwhite+NaOH, Au NCs solution microwaved for different time 1, 3, 5,10 minutes (a)under white light (b) under uv light representing red fluorescence after 3 minutes of microwave

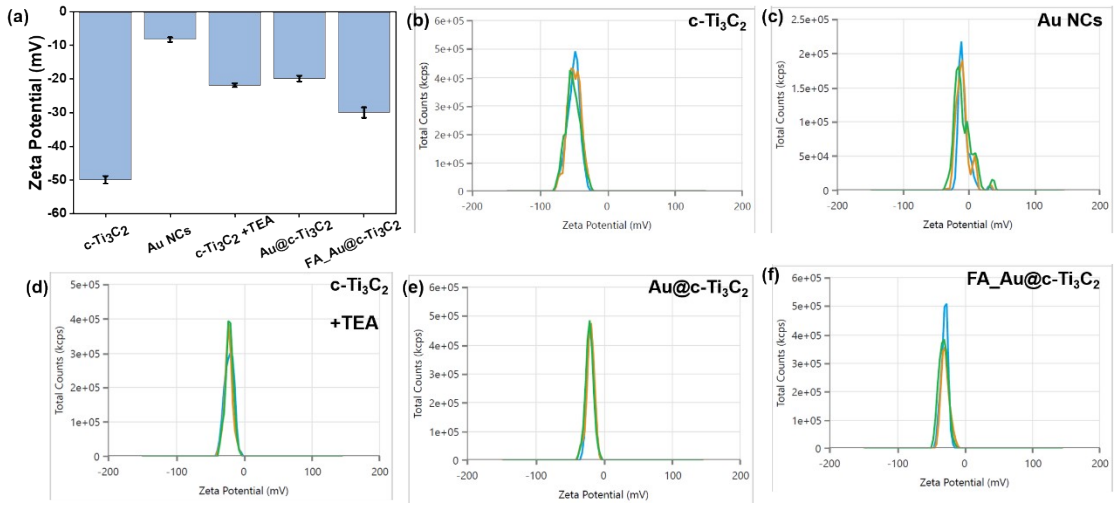

Figure S2: Zeta potential measurement of (a)Histogram (b) c-Ti_3C_2 (c)Au NCS (d) c-Ti_3C_2+TEA (e) Au@c_Ti_3C_2 (f) FA_A@c-Ti_3C_2

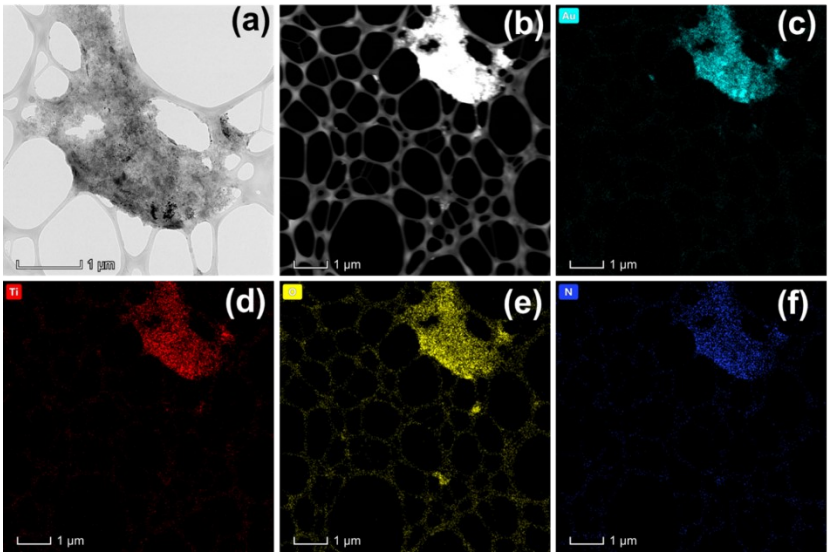

Figure S3: Morphological Characterization of Au@Ti_3C_2 (A) TEM Image (B) HAADF Image. Elemental Mapping Confirming Presence Of (C) Gold(Au) (D) Titanium (Ti) (E) Oxygen(O) (F) Nitrogen(N)

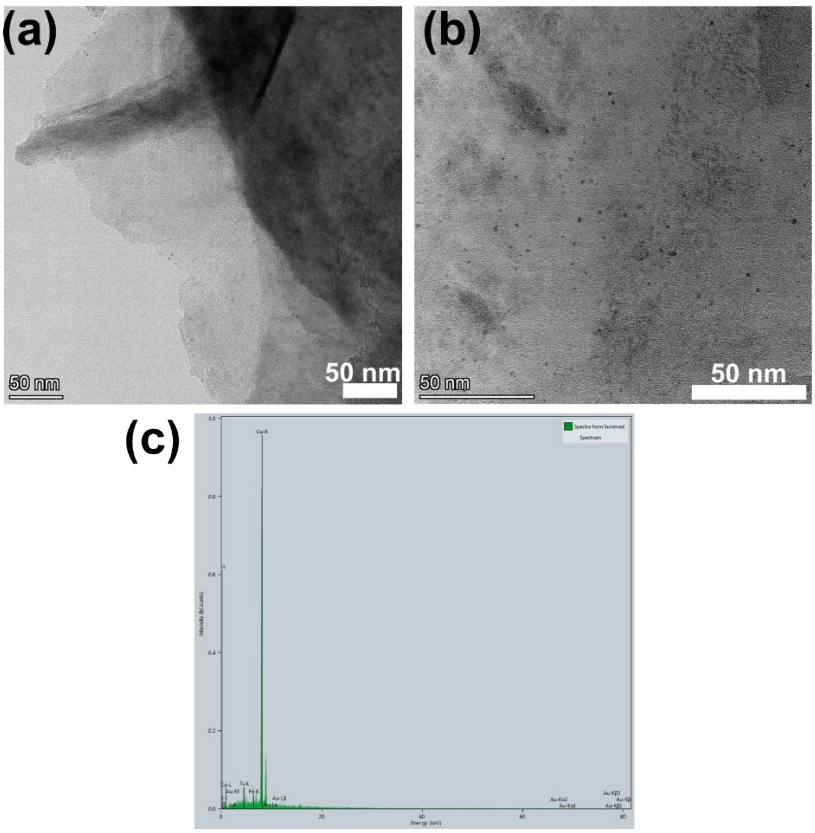

Figure S4 TEM images of Au NCs conjugation on flat Ti_3C_2 nanosheets (TMA^+_Ti_3C_2). (c) EDS of the sheets

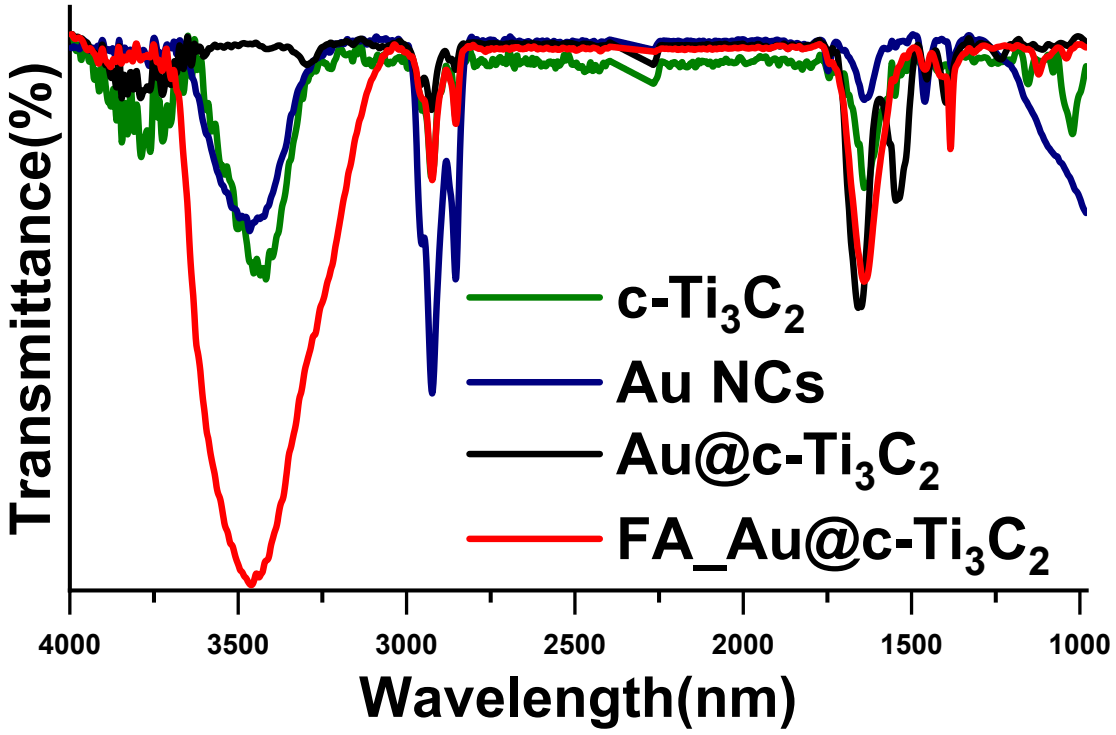

Figure S5: FTIR spectra of c-Ti_3C_2, Au NCs, Au @c-Ti_3C_2 and Fa_Au@c-Ti_3C_2

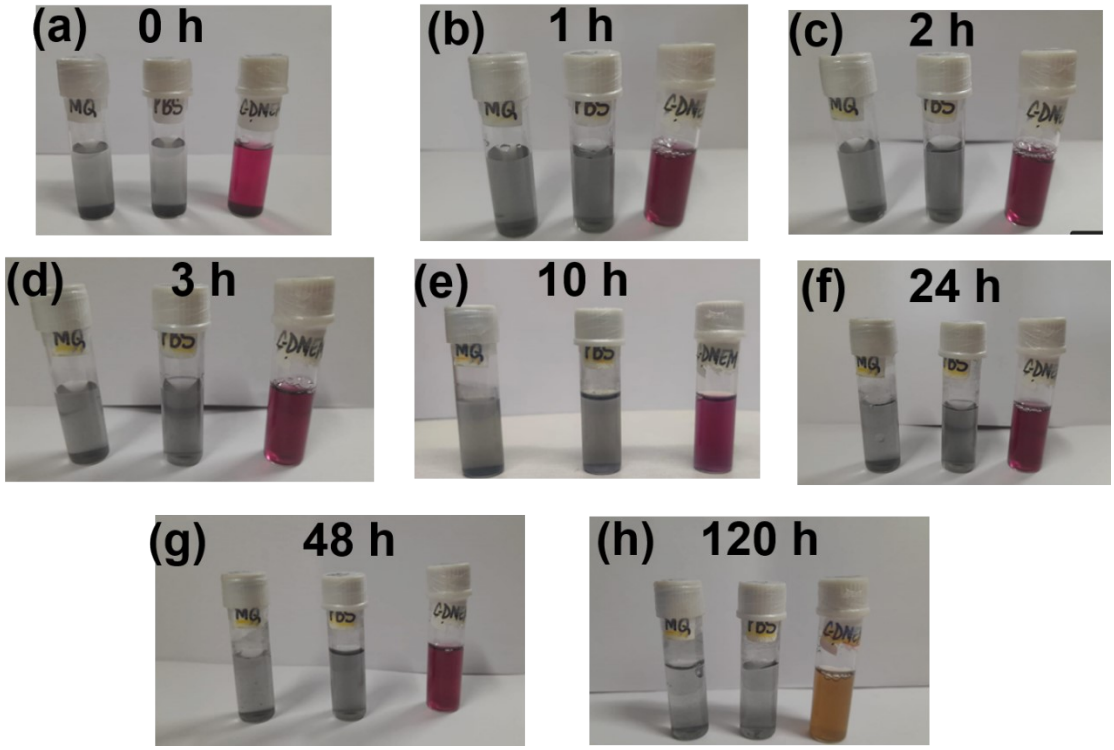

Figure S6 Digital images of FA_Au@c-Ti_3C_2 dispersed in Milli-Q, PBS and Complete DMEM at different time points to demonstrate its stability (a) 0 hour (b) 1 hour (c) 2 hours (d) 3 hours (e) 10 hours (f) 24 hours (g) 48 hours (h) 120 hours

In-vivo toxicity (Oral administration):

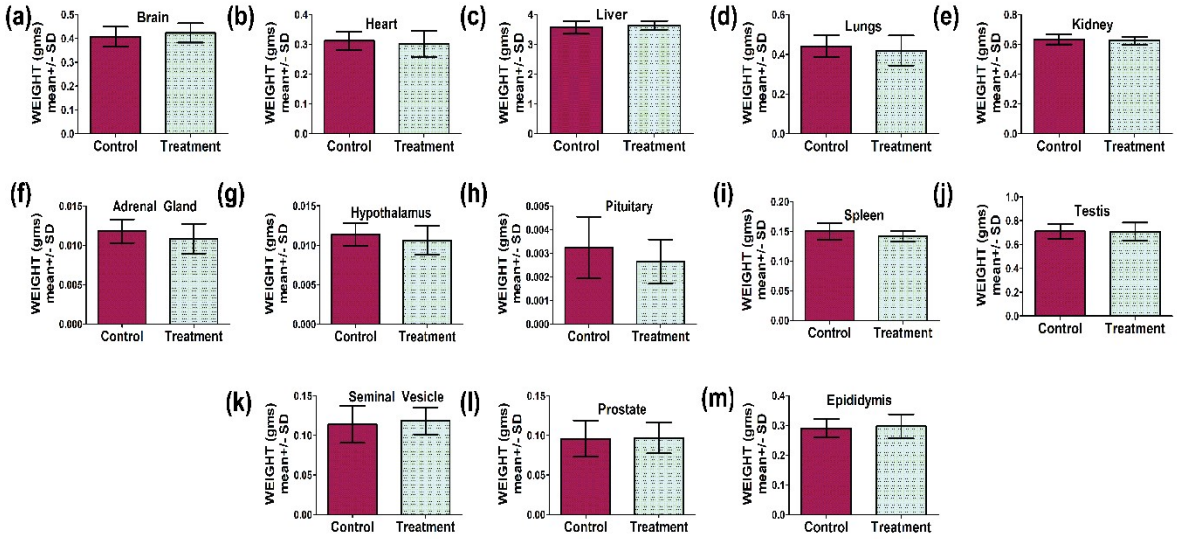

Figure S7: Individual body weight of various organs of oral administrated FA_Au@Ti_3C_2 treated male Wistar rats at day 14 administrated I.V. (a)brain (b) heart (c) liver (d) lungs (e)

kidney (f)adrenal gland (g) hypothalamus (h) pituitary (i) spleen (j) testis (k) seminal vesicles (l) prostate (m) epididymis

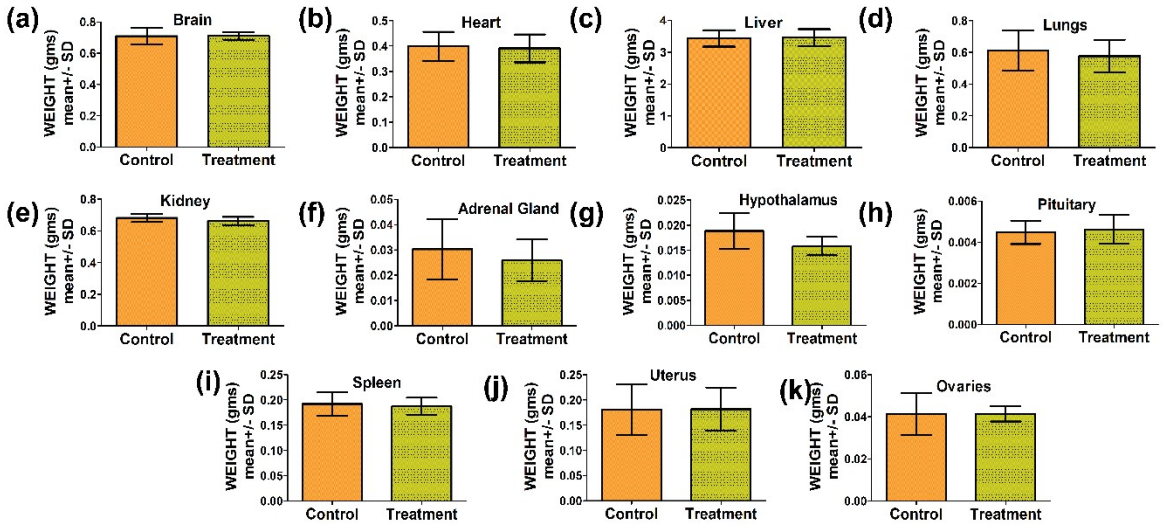

Figure S8: Individual body weight of various organs of oral administrated FA_Au@Ti_3C_2 treated female Wistar rats at day 14 (a)brain (b) heart (c) liver (d) lungs (e) kidney (f)adrenal gland (g) hypothalamus (h) pituitary (i) spleen (j) uterus (k) ovaries

In-vivo toxicity (I.V. administration):

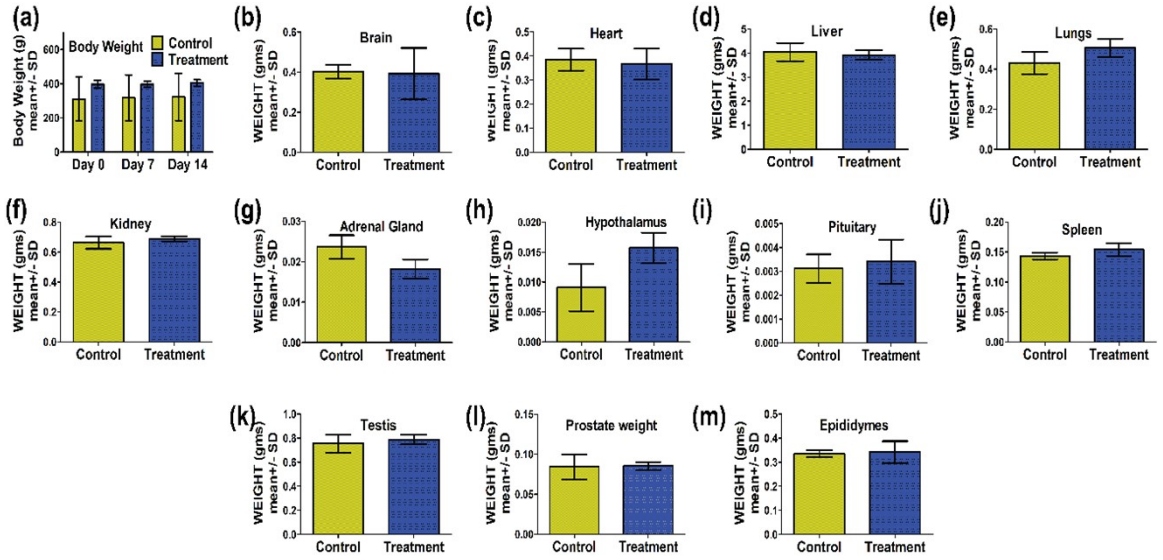

Figure S9: (a) comparative body weight of control and FA_Au@Ti_3C_2 treated male Wistar rats at 0day, 7th day and 14th day administrated I.V. Individual body weight of various organs at

day 14 (b) brain (c) heart (d) liver (e) lungs (f) kidney (g) adrenal gland (h) hypothalamus (i) pituitary (j) spleen (k) testis (l) prostate (m) epididymis

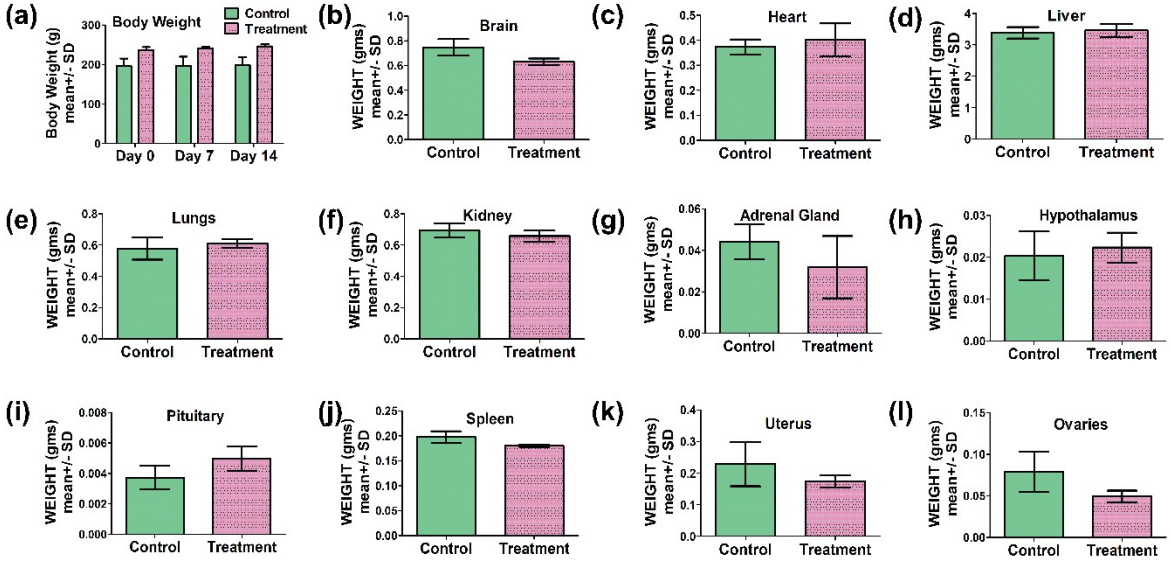

Figure S10: (a) comparative body weight of control and FA_Au@Ti_3C_2 treated female Wistar rats at 0-day, 7th day and 14th day administrated I.V. individual body weight of various organs at day 14 (b) brain (c) heart (d) liver (e) lungs (f) kidney (g) adrenal gland (h) hypothalamus (i) pituitary (j) spleen (k) uterus (l) ovaries

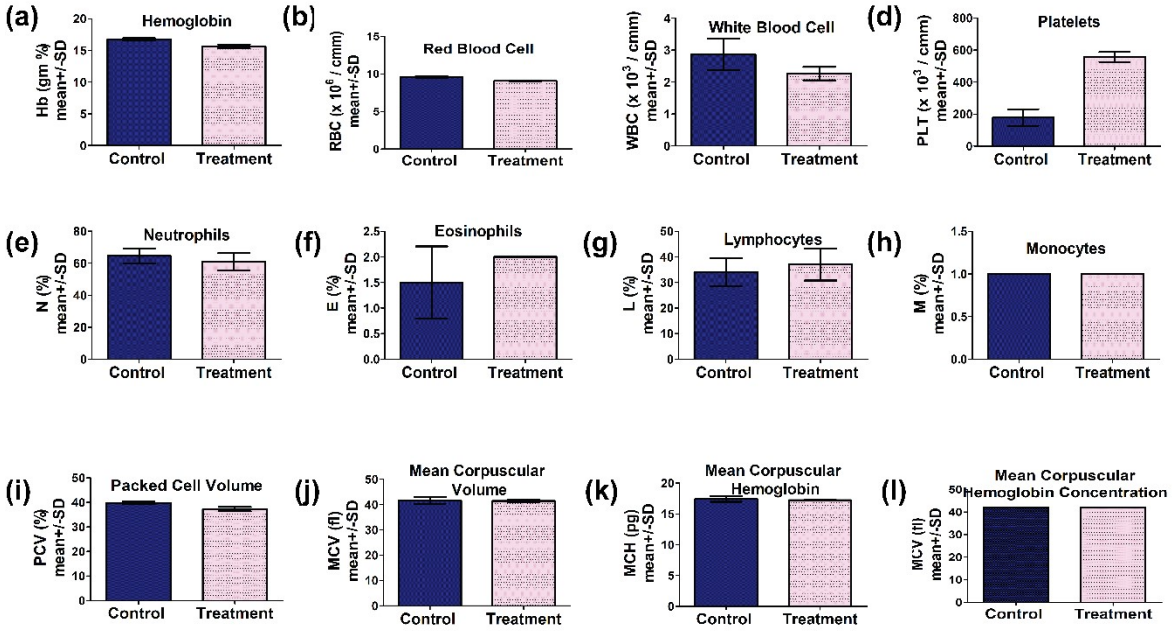

Figure S11: Hematology data of male wistar rats treated with FA_Au@Ti_3C_2 at the I.V. dose of 20 mg/kg (a) hemoglobin (b)Monocytes (c) white blood cells (d) platelets (e) neutrophils (f) eosinophils (j) lymphocytes (h) monocytes (i) packed cell volume (j) mean corpuscular volume (k)mean corpuscular hemoglobin (l) mean corpuscular hemoglobin concentration

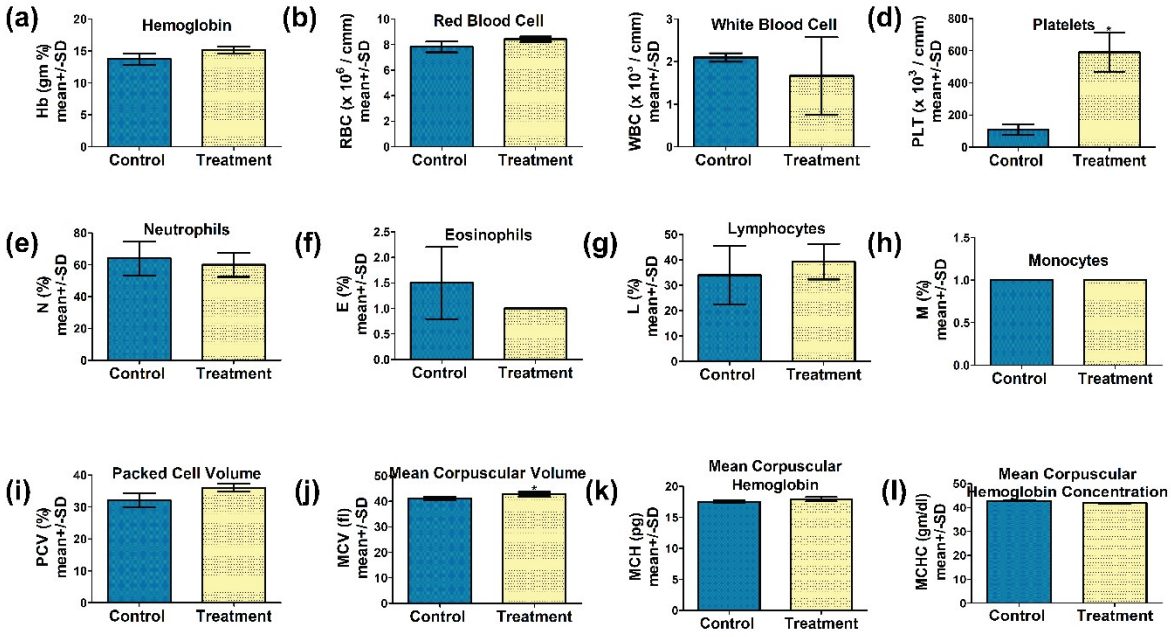

Figure S12: Hematology data of female wistar rats treated with FA_Au@Ti_3C_2 at the I.V. dose of 20 mg/kg (a) hemoglobin (b)red blood cells (c) white blood cells (d) platelets (e)neutrophils (f) eosinophils (j) lymphocytes (h) monocytes (i) packed cell volume (j) mean corpuscular volume (k)mean corpuscular hemoglobin (l) mean corpuscular hemoglobin concentration

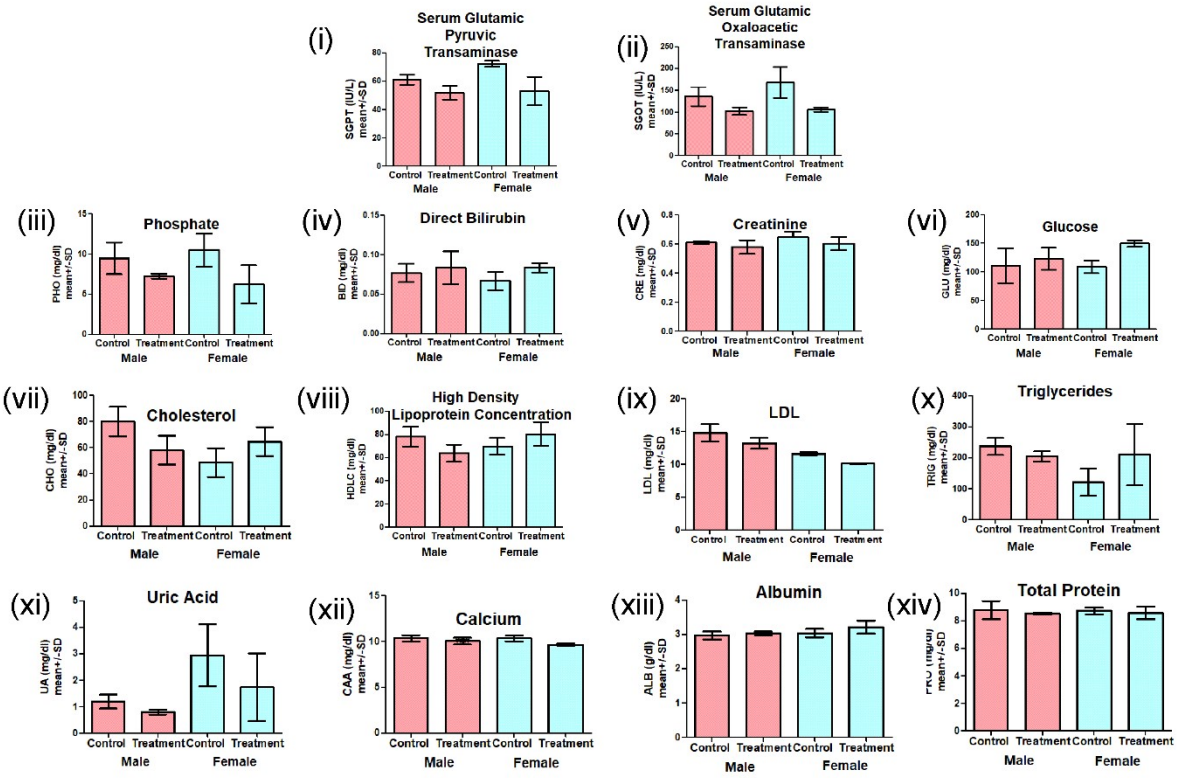

Figure S13 Serum biochemistry analysis (mean ± SD) of control and FA_Au@Ti_3C_2 treated male and female Wistar rats when administered via I.V. mode

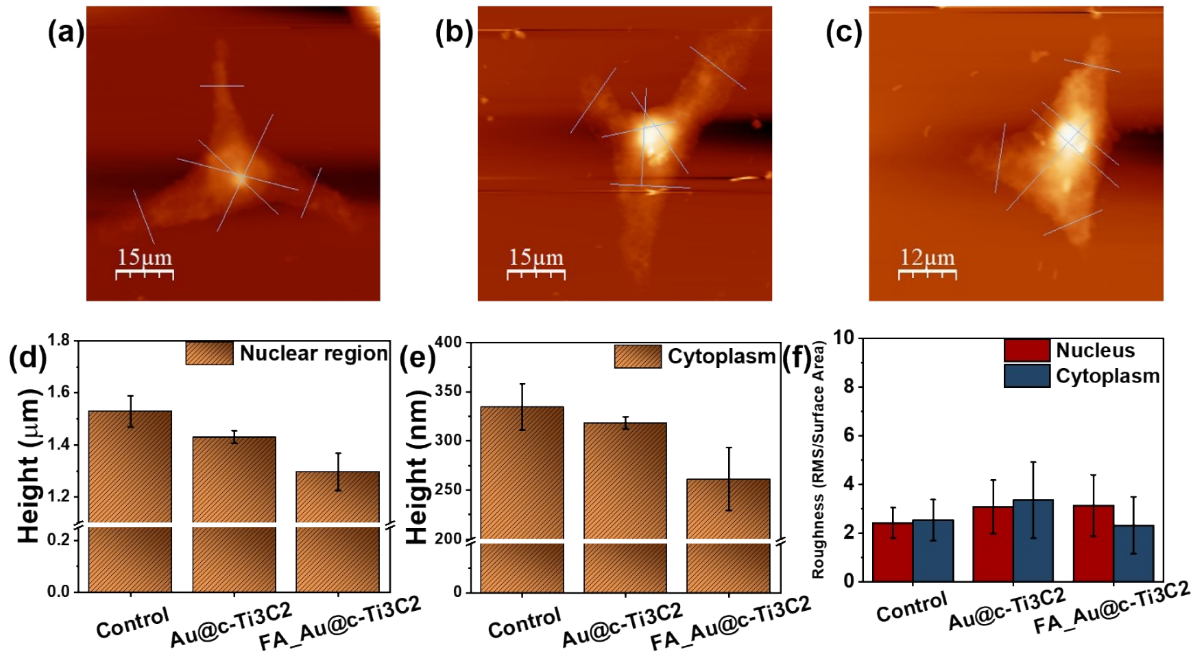

Figure S14: AFM images showing uptake of material (a) control MDAMB cells (b) cells treated with Au@c-Ti_3C_2 (c) cells treated with FA_Au@c-Ti_3C_2 (d) comparative height of the

nucleus region of cells (e) comparative height of the cytoplasm of cells (f) comparative roughness of the cell surface at nucleus and cytoplasm region.

Photothermal conversion efficiency (PCE):

Plasmonic metallic nanostructures may absorb light and convert it to heat, which is then conveyed to the surrounding environment, causing a temperature rise. The photothermal conversion efficiency is a significant component in the effective usage of plasmonic nanostructures in all of these applications. Several approaches for characterizing the photothermal conversion effect have been developed. The photothermal conversion characteristics of nanocrystals may be measured by directly monitoring temperature increases under laser irradiation using a thermocouple placed in the aqueous nanocrystal dispersions. This direct measuring approach is simple and straightforward[10,11].

Total energy balance of the system[11,12] is expressed by the following equation (1)

$$\sum_i m_i C_{p,i} \frac{dT}{dt} = Q_{NS} + Q_{Dis} - Q_{Surr} \qquad \text{----------Eq. 1}$$

Where m = water mass, Cp = water heat capacity, T = solution temperature Q_{NS} = nanostructures' energy input, Q_{Dis} is the sample cell's baseline energy input, and Q_{Surr} is the heat conduction from the system surface via air.

The laser induced source term, Q_{NS}, describes the heat released from the surface during NIR laser irradiation of nanostructures.

$$Q_{NS} = I\left(1 - 10^{-A_{laser\ wavelength}}\right)\eta \qquad \text{----------Eq. 2}$$

Where, I is incident laser power, η is the conversion efficiency, and $A_{laser\ wavelength}$ is the nanostructure absorbance at NIR laser.

Q_{Surr} is the emitted thermal energy and is given by the equation below.

$$Q_{Surr} = hS(T - T_{Surr}) \qquad \text{----------Eq. 3}$$

where h is the heat transfer coefficient, S is the well's surface area, T is the solution temperature, and T_{Surr} is the surrounding temperature.

Because the heat output Q_{Surr} increases with the increase in temperature (Eq. 3), the system temperature will reach a maximum when the heat input equals the heat output, as illustrated in the following equation (Eq. 4).

$$Q_{NS} + Q_{Dis} = Q_{Surr-Max} = hS(T_{Max} - T_{Surr}) \quad \text{----------Eq. 4}$$

When the sample cell achieves the equilibrium temperature, $Q_{Surr\text{-}Max}$ represents heat conduction away from the system, and T_{Max} represents the equilibrium temperature.

Photothermal transduction efficiency η can be calculated by substituting equation (2) for Q_{NS} into equation (4) and obtaining equation (5)

$$\eta = \frac{hS(T_{Max} - T_{Surr}) - Q_{Dis}}{I(1 - 10^{-A_{laser\ wavelength}})} \quad \text{----------Eq. 5}$$

Where Q_{Dis} was measured separately using water. As a result, only the hS is unknown for calculating η. The highest system temperature T_{Max} is used to calculate hS by introducing θ which is a dimensionless driving force temperature.

$$\theta = \frac{T - T_{Surr}}{T_{Max} - T_{Surr}} \quad \text{----------Eq. 6}$$

And a sample system time constant τ_s

$$\tau_s = \frac{\sum_i m_i C_{p,i}}{hS} \quad \text{----------Eq. 7}$$

which is substituted into equation (1) and rearranged to yield

$$\frac{d\theta}{dt} = \frac{1}{\tau_s}\left[\frac{Q_{NS} + Q_{Dis}}{hS(T_{Max} - T_{Surr})} - \theta\right] \quad \text{----------Eq. 8}$$

When the laser source is turned off, $Q_{NS} + Q_{Dis} = 0$, thereby reducing the equation (4) to

$$\frac{d\theta}{dt} = \frac{-\theta}{\tau_s} \quad \text{----------Eq. 9}$$

and after integration, giving the expression

$$t = -\tau_s ln\theta \quad \text{----------Eq. 10}$$

As a result, the time constant *(τs)* was calculated by graphing time vs the negative logarithm of temperature throughout the cooling phase.

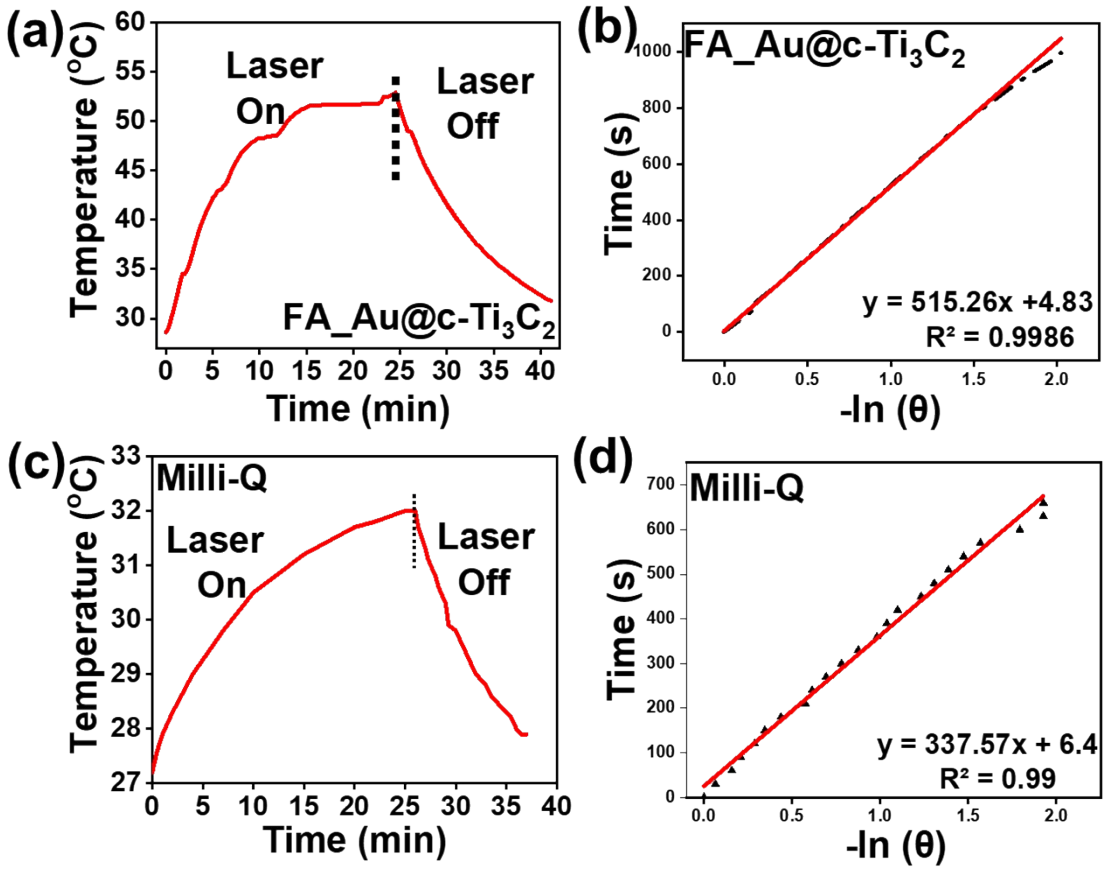

Figure S15: (a) Change in temperature corresponding to Laser ON and OFF when FA_Au@c-Ti_3C_2 was irradiated using 808 nm laser. (b) Time versus negative logarithm plot from cooling stage. (a) Change in temperature corresponding to Laser ON and OFF when Milli-Q was irradiated using 808 nm laser. (b) Time versus negative logarithm plot from cooling stage.

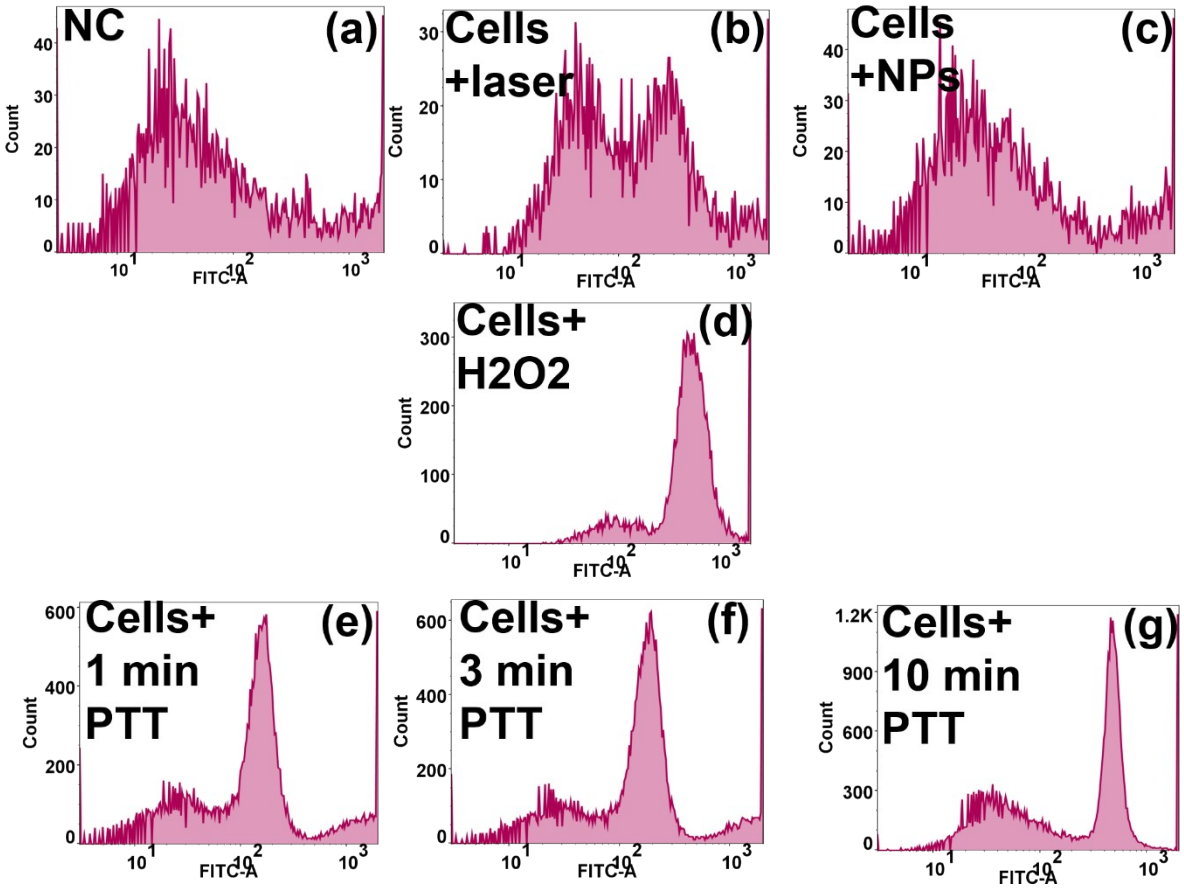

Figure S16 DCFDA assay performed on MDAMB cell line to identify ROS generation (a) Negative control/Untreated cells (b) Cells treated with 808nm laser (c) cells treated with FA_Au@c-Ti_3C_2 (d) Cells treated with H_2O_2 (positive control) (e) PTT treatment for 1 minutes (f) PTT treatment for 3 minutes (g) PTT treatment for 10 minutes using FA_Au@c-Ti_3C_2.

References:

(1) Thakur, M.; Gupta, H.; Singh, D.; Mohanty, I. R.; Maheswari, U.; Vanage, G.; Joshi, D. Histopathological and Ultra Structural Effects of Nanoparticles on Rat Testis Following 90 Days (Chronic Study) of Repeated Oral Administration. *J. Nanobiotechnology* **2014**, *12* (1), 1–13. https://doi.org/10.1186/s12951-014-0042-8.

(2) Mohammadniaei, M.; Koyappayil, A.; Sun, Y.; Min, J.; Lee, M. H. Gold Nanoparticle/MXene for Multiple and Sensitive Detection of OncomiRs Based on Synergetic Signal Amplification. *Biosens. Bioelectron.* **2020**, *159*, 112208. https://doi.org/10.1016/j.bios.2020.112208.

(3) Tang, W.; Dong, Z.; Zhang, R.; Yi, X.; Yang, K.; Jin, M.; Yuan, C.; Xiao, Z.; Liu, Z.; Cheng, L. Multifunctional Two-Dimensional Core-Shell MXene@Gold Nanocomposites for Enhanced Photo-Radio Combined Therapy in the Second Biological Window. *ACS Nano* **2019**, *13* (1), 284–294. https://doi.org/10.1021/acsnano.8b05982.

(4) Zheng, K.; Li, S.; Jing, L.; Chen, P. Y.; Xie, J. Synergistic Antimicrobial Titanium Carbide (MXene) Conjugated with Gold Nanoclusters. *Adv. Healthc. Mater.* **2020**, *9* (19), 2001007. https://doi.org/10.1002/adhm.202001007.

(5) Xie, H.; Li, P.; Shao, J.; Huang, H.; Chen, Y.; Jiang, Z.; Chu, P. K.; Yu, X. F. Electrostatic Self-Assembly of Ti3C2Tx MXene and Gold Nanorods as an Efficient Surface-Enhanced Raman Scattering Platform for Reliable and High-Sensitivity Determination of Organic Pollutants. *ACS Sensors* **2019**, *4* (9), 2303–2310. https://doi.org/10.1021/acssensors.9b00778.

(6) Boularaoui, S.; Shanti, A.; Lanotte, M.; Luo, S.; Bawazir, S.; Lee, S.; Christoforou, N.; Khan, K. A.; Stefanini, C. Nanocomposite Conductive Bioinks Based on Low-Concentration GelMA and MXene Nanosheets/Gold Nanoparticles Providing Enhanced Printability of Functional Skeletal Muscle Tissues. *ACS Biomater. Sci. Eng.* **2021**, *7* (12), 5810–5822. https://doi.org/10.1021/acsbiomaterials.1c01193.

(7) Elumalai, S.; Mani, V.; Jeromiyas, N.; Ponnusamy, V. K.; Yoshimura, M. A Composite Film Prepared from Titanium Carbide Ti3C2Tx (MXene) and Gold Nanoparticles for Voltammetric Determination of Uric Acid and Folic Acid. *Microchim. Acta* **2020**, *187* (1), 1–10. https://doi.org/10.1007/s00604-019-4018-0.

(8) Satheeshkumar, E.; Makaryan, T.; Melikyan, A.; Minassian, H.; Gogotsi, Y.; Yoshimura, M. One-Step Solution Processing of Ag, Au and Pd@MXene Hybrids for SERS. *Sci. Rep.* **2016**, *6* (1), 1–9. https://doi.org/10.1038/srep32049.

(9) Hussein, E. A.; Zagho, M. M.; Rizeq, B. R.; Younes, N. N.; Pintus, G.; Mahmoud, K. A.; Nasrallah, G. K.; Elzatahry, A. A. Plasmonic MXene-Based Nanocomposites Exhibiting Photothermal Therapeutic Effects with Lower Acute Toxicity than Pure MXene. *Int. J. Nanomedicine* **2019**, *14*, 4529–4539. https://doi.org/10.2147/IJN.S202208.

(10) Chen, H.; Shao, L.; Ming, T.; Sun, Z.; Zhao, C.; Yang, B.; Wang, J. Understanding the Photothermal Conversion Efficiency of Gold Nanocrystals. *Small* **2010**, *6* (20), 2272–2280. https://doi.org/10.1002/smll.201001109.

(11) Roper, D. K.; Ahn, W.; Hoepfner, M. Microscale Heat Transfer Transduced by Surface Plasmon Resonant Gold Nanoparticles. *J. Phys. Chem. C* **2007**, *111* (9), 3636–3641. https://doi.org/10.1021/jp064341w.

(12) Liu, X.; Li, B.; Fu, F.; Xu, K.; Zou, R.; Wang, Q.; Zhang, B.; Chen, Z.; Hu, J. Facile Synthesis of Biocompatible Cysteine-Coated CuS Nanoparticles with High Photothermal Conversion Efficiency for Cancer Therapy. *Dalt. Trans.* **2014**, *43* (30), 11709–11715. https://doi.org/10.1039/c4dt00424h.